A Coupled Resonator Decoupling Network for Two-Element Compact Antenna Arrays in Mobile Terminals

Luyu Zhao, *Member, IEEE*, Lap K. Yeung, *Member, IEEE*, and Ke-Li Wu, *Fellow, IEEE*

***Abstract*—A new concept for decoupling two coupled antenna elements in a broad band using a coupled resonator decoupling network (CRDN) is proposed for the first time. A synthesis and design theory of a CRDN is presented. Based on the admittance parameters of a given antenna array, a set of required rational functions and, consequently, the coupling matrix for a second-order decoupling network is obtained analytically. To prove the concept, two prototypes using microstrip resonators are designed and experimentally studied. Measurement results have demonstrated that an isolation improvement of more than 10 dB can be achieved within more than 15% bandwidth in both examples. The benefits of using a CRDN for different levels of isolation in a MIMO terminal are investigated through experiments and simulations. The results have shown that, as compared to the existing decoupling scheme using a lumped element, the proposed CRDN scheme can significantly increase the radiation efficiency, reduce the correlation, improve the channel capacity, and above all enhance the throughput of a MIMO terminal. The technique is general and can be applied to both symmetric and asymmetric arrays.**

***Index Terms*—Compact antenna array, decoupling network, multiple-input multiple-output (MIMO), mutual coupling, network synthesis.**

I. Introduction

With the increasing demands on higher data rate, greater spectrum efficiency, larger average throughput and shorter latency by wireless systems, many advanced technologies have been developed to confront the challenges. Among them, orthogonal frequency division multiplex (OFDM) and multiple-input multiple-output (MIMO) are two important enabling technologies that have received tremendous attention in both industry and academic community. OFDM uses multiple sub-carriers that are multiplexed in a wide frequency spectrum, whereas MIMO provides a way of utilizing the multiple signal paths that exist between a transmitter and a receiver to significantly improve the data throughput on a given radio channel [1]. By using multiple antennas at a transmitter and a receiver along with some complex signal processing techniques, MIMO technology enables the system to set up parallel data streams on a single channel, thereby increasing the channel capacity by several times [2]. Therefore, wideband transmitting and receiving multiple antenna arrays have become indispensable in an advanced wireless communication system.

When a multiple antenna system is implemented in a mobile terminal, the array elements have to be contained in a compact volume, which results in large pattern/spatial correlation and strong mutual coupling between the elements. The channel capacity decreases as the correlation increases. Additionally, if mutual coupling is strong, a large portion of the power fed into one port will be coupled to the other port rather than radiating to free space, and thus reducing the signal-to-noise ratio, the radiation efficiency and eventually deteriorating the channel capacity. All of these degradations diminish the benefits of a multiple antenna system. Therefore, developing an effective decoupling technology has become a focused research area in recent years.

Various decoupling schemes have been proposed, which can be divided into four major categories:

1) Eigen-Mode Decomposition Scheme: Its principle is to diagonalize the scattering matrix of a compact array using 90° and/or 180° hybrids. The scheme can be applied to coupled monopoles [3], loop antennas [4], and mobile phone antennas that use the chassis as the main radiator [5]. A systematic design procedure exists and can be applied to any symmetric array [6]. Moreover, by making use of the orthogonal modes, mode-based beam steering can be achieved [7]. These eigenmodes, however, have significantly different matching bandwidth and efficiency. In fact, some of the high Q modes may have an impractically narrow bandwidth.

2) The Inserted Component Scheme: In the 1970's, Andersen [8] proposed a necessary condition for the occurrence of no coupling between antennas and proved the concept by inserting a section of transmission-line between the coupled antenna ports. The limitation is that the antenna spacing has to be fixed to certain values. A lumped element connected in shunt with the coupled antennas can also achieve certain level of isolation [9], [10]. Such decoupling schemes overcome some major shortcomings of [8] and can be considered as a decoupling network of zeroth-order with relatively narrow decoupling bandwidth, which causes high sensitivity to the surroundings of the antennas in close proximity such as human hands. Recently, a neutralization line technique was proposed for decoupling two antennas [11]–[13]. The line not only creates a second path of cur-

Manuscript received September 09, 2013; revised December 25, 2013; accepted February 07, 2014. Date of publication February 26, 2014; date of current version May 01, 2014. This work was supported in part by University Grants Committee of Hong Kong under Grant AoE/P-04/08 and also in part by Development and Reform Commission of Shenzhen Municipality under Grant Shen Fa Gai (2013) 1673.

The authors are with the Department of Electronic Engineering, The Chinese University of Hong Kong, Shatin, NT, Hong Kong (e-mail: lyzhao@ee.cuhk.edu.hk; lkyeung@ee.cuhk.edu.hk; klwu@ee.cuhk.edu.hk).

Color versions of one or more of the figures in this paper are available online at http://ieeexplore.ieee.org.

Digital Object Identifier 10.1109/TAP.2014.2308547

rent flow but also perturbs the radiated fields. Existing designs are carried out intuitively and are antenna dependent.

3) Artificial Structure Decoupling Scheme: This scheme involves the use of sub-wavelength EM structures such as mushroom-like electromagnetic band gap (EBG) structures [14], defected ground structures (DGS) [15], and magnetic metamaterials [16]. These structures provide bandstop filtering characteristics at certain extent. A common issue for these structures is that they are all *ad hoc* to particular antennas and their footprints are large. Another similar narrow band approach is to use a parasitic scatter/radiator [17].

4) Coupled Resonator Decoupling Scheme: A preliminary result of decoupling a pair of coupled elements using a second-order coupled resonator network was reported in 2012 by the authors [18], in which not only the sequential but also a cross couplings are introduced for a broadband decoupling performance. Nevertheless, a thorough investigation both theoretically and experimentally is needed.

This paper systematically presents the general concept of a coupled resonator decoupling network (CRDN). Compared to the existing decoupling techniques, the proposed decoupling network possess the following unique features: 1) it provides a higher-order and wideband decoupling solution; 2) it offers a tradeoff between decoupling bandwidth and degree of isolation; 3) it is relatively antenna independent and can be realized using a wide selection of manufacturing technologies; 4) it can be applied to multiple antenna problems [19]; and 5) it can be designed using existing filter design theory and realization techniques.

The synthesis and design theory of a general CRDN starts from the decoupling and matching conditions of admittance parameters. The detailed procedures for synthesizing the required polynomials that lead to the coupling coefficients of a CRDN will be elaborated. For illustration, the design processes for two practical compact antenna arrays are presented. Although the CRDNs used in these two examples are implemented by microstrip resonators, they can also be implemented by various other means, such as low temperature co-fired ceramics (LTCC) and silicon-based integrated passive device (IPD) technologies. The working mechanism of the CRDN is revealed by comparing simulated current distributions of a decoupled array and its coupled counterpart. The antenna dependency issue is also discussed in detail. To give a full picture of the CRDN, several important figures of merits for mobile terminals, such as isolation, radiation efficiency, envelope correlation coefficient (ECC), channel capacity, and throughput are investigated. A decoupled array using a lumped element network [9] is also studied for comparison purpose. The measurement results demonstrated the promising potentials of the proposed technique for MIMO and other multiple antenna systems.

II. Synthesis of a CRDN

A. Decoupling and Matching Conditions

It is assumed that a pair of coupled antennas is represented by a 2-by-2 admittance matrix ($\mathbf{Y}^A$) with complex entries. For the decoupling configuration shown in Fig. 1, the decoupling network consisting of a series of coupled resonators (i.e. CRDN)

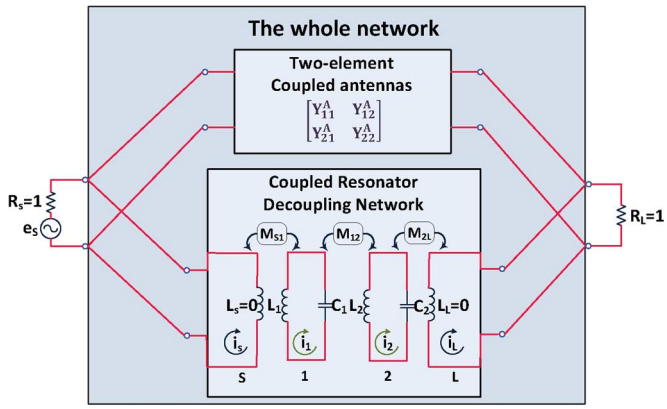

Fig. 1. Network representation of two coupled antennas in shunt with a CRDN.

is connected in parallel to the pair of coupled antennas. The two matched ports of the decoupled system are terminated by two unit loads. Assuming the CRDN is lossless, the entries in its admittance matrix $\mathbf{Y}^F$ are all purely imaginary. Obviously, the total admittance is the sum of the two individual admittance matrices as

$$\mathbf{Y} = \begin{bmatrix} Y_{11} & Y_{12} \\ Y_{21} & Y_{22} \end{bmatrix} = \begin{bmatrix} Y_{11}^A + Y_{11}^F & Y_{12}^A + Y_{12}^F \\ Y_{21}^A + Y_{21}^F & Y_{22}^A + Y_{22}^F \end{bmatrix}. \quad (1)$$

Notice that the overall network is reciprocal but not necessarily symmetric. It can be easily obtained from an S-to-Y transformation that the two ports will be well isolated within a given frequency range if

$$Y_{21}(\omega_B) = Y_{21}^A(\omega_B) + Y_{21}^F(\omega_B) \approx 0 \quad (2)$$

where ω_B is the radian frequency. Since Y_{21}^F is imaginary, (2) implies the following two decoupling conditions:

$$\mathrm{Re}\left\{Y_{21}^A(\omega_B)\right\} \approx 0 \quad (3a)$$

and

$$j \cdot \mathrm{Im}\left\{Y_{21}^A(\omega_B)\right\} + Y_{21}^F(\omega_B) \approx 0. \quad (3b)$$

Having had (3) satisfied, it is clear that

$$S_{11} \approx \frac{1 - Y_{11}^A - Y_{11}^F}{1 + Y_{11}^A + Y_{11}^F}, \text{ and } S_{22} \approx \frac{1 - Y_{22}^A - Y_{22}^F}{1 + Y_{22}^A + Y_{22}^F} \quad (4)$$

from which the matching conditions can be obtained as

$$\mathrm{Re}\left\{Y_{kk}^A(\omega_B)\right\} \approx 1, \quad k = 1, 2, \quad (5a)$$

$$j \cdot \mathrm{Im}\left\{Y_{kk}^A(\omega_B)\right\} + Y_{kk}^F(\omega_B) \approx 0, \quad k = 1, 2. \quad (5b)$$

B. Admittance Transformation

Supposing that the coupled antenna array is matched to a real reference load (Z_0), condition (3a) can be realized at the center frequency by inserting a piece of transmission line with electrical length θ and characteristic impedance Z_0 at each antenna port. Assuming the $|S_{21}|e^{j\phi_{21}}$ of the original antenna array to be a complex number in general, then [9]

$$\theta = \frac{1}{2}\left(\phi_{21} - \frac{\pi}{2} \pm k\pi\right), \quad k = 0, 1, 2 \ldots. \quad (6)$$

C. Synthesis of Decoupling Network

The concept of coupling matrix, which is developed for designing bandpass filters, can be applied to describe a CRDN as shown in Fig. 1. The design process of this network starts with synthesizing the rational functions for the admittance parameters using the requirements imposed by (3) and (5). For a second-order CRDN without finite transmission zeroes, the mutual admittance can be expressed as

$$Y_{21}^F(s) = \frac{j\gamma}{(s-jp_1)(s-jp_2)} \tag{7}$$

where γ, p_1, and p_2 are real constants, and $s = \sigma + j\omega$ is the complex frequency variable defined in the lowpass frequency domain. Without loss of generality, it is assumed that $p_1 < p_2$. It is worth mentioning that for the lowpass prototype circuit (LPC) of a coupled resonator network, the rational function $Y_{21}^F(s)$ is not necessarily a quotient of even to odd or odd to even polynomials. This is because frequency invariant reactances (FIRs) and an extra inverter element are introduced in the second-order LPC [20]. It can be shown that with appropriate approximation in converting the rational function to a network realization, the resultant network will be a quotient of even to odd or odd to even polynomials. Furthermore, $Y_{21}^F(s)$ may not be positive real [21].

The partial fractional expansion of (7) can be re-expressed as

$$Y_{21}^F(s) = \frac{r_1^{21}}{s-jp_1} + \frac{r_2^{21}}{s-jp_2} \tag{8}$$

where residues $r_1^{21} = \gamma/(p_1 - p_2)$ and $r_2^{21} = \gamma/(p_2 - p_1)$. Notice that the two residues of $Y_{21}^F(s)$ must be real but with opposite signs. In general, the residues of $Y_{11}^F(s)$ and $Y_{22}^F(s)$ can be obtained through [20]

$$\sqrt{r_k^{11} \cdot r_k^{22}} = \pm r_k^{21}, \quad k = 1, 2. \tag{9}$$

Based on the residues of $Y_{21}^F(s)$, a proper sign in (9) can be chosen. For a realizable passive network, $Y_{11}^F(s)$ and $Y_{22}^F(s)$ must be positive real [21]. Then to find the rational functions $Y_{11}^F(s)$ and $Y_{22}^F(s)$ from (9), two positive scaling coefficients c and d need to be introduced so that

$$\begin{aligned} r_1^{11} &= c \cdot \left|r_1^{21}\right| = \frac{c|\gamma|}{(p_2-p_1)},\ r_2^{11} = d \cdot \left|r_1^{21}\right| = \frac{d|\gamma|}{(p_2-p_1)}, \\ r_1^{22} &= \frac{1}{c} \cdot \left|r_2^{21}\right| = \frac{|\gamma|}{c(p_2-p_1)},\ r_2^{22} = \frac{1}{d} \cdot \left|r_2^{21}\right| = \frac{|\gamma|}{d(p_2-p_1)}. \end{aligned} \tag{10}$$

The absolute signs in (10) ensure $Y_{11}^F(s)$ and $Y_{22}^F(s)$ to be positive real. Therefore, the rational functions $Y_{11}^F(s)$ and $Y_{22}^F(s)$ can now be expressed as

$$Y_{11}^F(s) = \frac{c|\gamma|}{(s-jp_1)(p_2-p_1)} + \frac{d|\gamma|}{(s-jp_1)(p_2-p_1)} \tag{11a}$$

$$Y_{22}^F(s) = \frac{|\gamma|}{c(s-jp_1)(p_2-p_1)} + \frac{|\gamma|}{d(s-jp_1)(p_2-p_1)}. \tag{11b}$$

By substituting (8) and (11) into (3b) and (5b), parameters γ, p_1, p_2, c, and d can be determined analytically and the transversal $N+2$ coupling matrix for the decoupling network can then be synthesized by following the procedure given in [20]. To obtain the coupling matrix for a folded coupling structure, a matrix similarity transformation with pivot (2, 3) can be applied. The transformed coupling matrix can be analytically expressed by

$$\begin{aligned} m_{s1} &= \sqrt{\frac{|\gamma| \cdot (c+d)}{(p_2-p_1)}}, \quad m_{2L} = \sqrt{\frac{|\gamma| \cdot (c+d)}{cd \cdot (p_2-p_1)}} \\ m_{12} &= \frac{\gamma}{|\gamma|}\sqrt{\frac{d}{c}} \cdot \frac{c}{c+d} \cdot (p_2-p_1), \quad m_{11} = \frac{-(cp_1+dp_2)}{c+d} \\ m_{22} &= \frac{-(cp_2+dp_1)}{c+d}, \quad m_{SL} = 0. \end{aligned} \tag{12}$$

where m_{S1}, m_{2L}, and m_{SL} are the coupling coefficients between source to resonator 1, resonator 2 to load, and source to load, respectively. Entries m_{11} and m_{22} are the self-couplings of resonator 1 and resonator 2, where $m_{ii} = -2\Delta\omega_{ii}/\omega_0$ that is proportional to the frequency shift of the resonator $\Delta\omega_{ii}$ w.r.t. the center frequency ω_0.

For a symmetrical decoupling network, $c = d = 1$ and $-p_1 = p_2 = p$, the coupling matrix can be simplified to

$$m_{s1} = m_{L2} = \sqrt{\frac{|\gamma|}{p}},\ m_{12} = \frac{\gamma p}{|\gamma|}\ m_{11} = m_{22} = 0,\ m_{SL} = 0. \tag{13}$$

It will be shown later that parameter p needs to be as large as the manufacturing process allows. The sign of $\gamma/|\gamma|$ must be opposite to that of the imaginary part of Y_{21}^A. It can be seen from (12) and (13) that to accommodate different couplings of coupled antennas, only input/output couplings need to be adjusted.

D. Design of Decoupling Network

In order to determine parameters γ, p_1, p_2, c, and d and obtain the coupling coefficients, the admittance parameters of the coupled antennas are transformed to the lowpass frequency domain with reference to unit terminations and designated fractional bandwidth (FBW) by

$$\omega = \frac{1}{\mathrm{FBW}}\left(\frac{\omega_B}{\omega_0} - \frac{\omega_0}{\omega_B}\right) \tag{14}$$

where ω_0 is the center frequency in the bandpass domain.

To illustrate the design procedure, a compact antenna array working at 2.6 GHz as shown in Fig. 2(a) is considered. The array is composed of one cone-shaped monopole and one meandered monopole. The center-to-center distance between the two elements D is 16.55 mm $(0.14\lambda_0)$ and the edge-to-edge distance S is 3.9 mm $(0.03\lambda_0)$. The simulated and the measured S-parameters are shown in Fig. 2(b).

It has been found by simulation and measurement that for many types of practical coupled antenna pairs, such as coupled PIFAs, monopoles, or patches, the imaginary part of Y_{21}^A is almost constant over a frequency range in the vicinity of resonance. In order to satisfy (3b), Y_{21}^F is desired to be relatively constant within the band of interest. In other words, because the

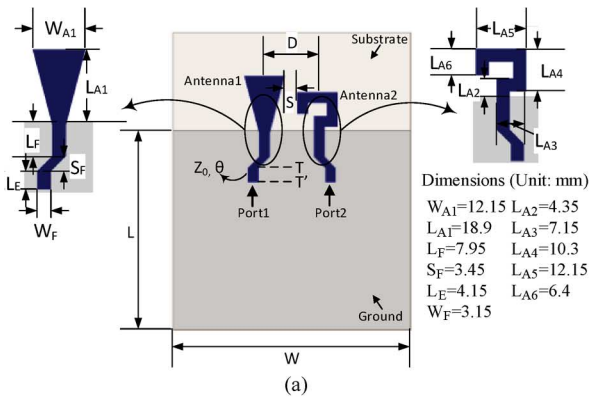

(a)

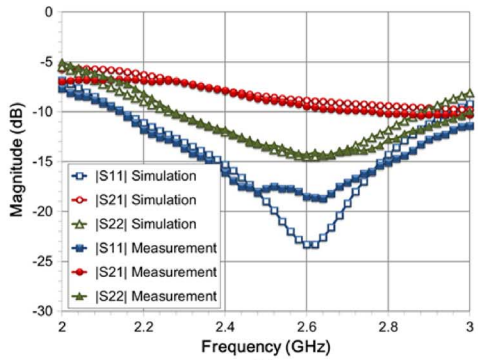

(b)

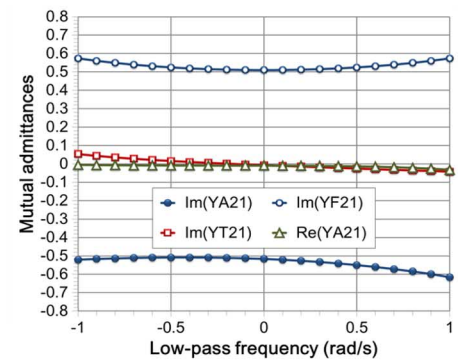

(c)

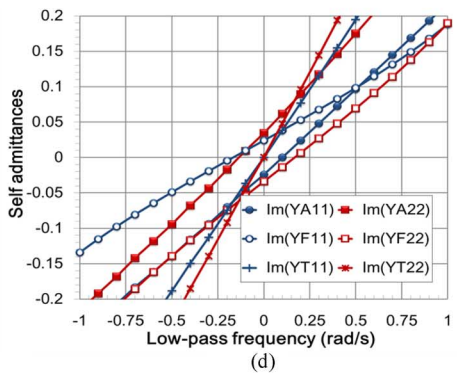

(d)

Fig. 2. (a) Asymmetric two-element compact array. (b) Simulated and measured S-parameter of the array. (c) Simulated Y_{21} of the array and a CRDN. (d) Simulated normalized Y_{11} and Y_{22} of the array and a CRDN.

slope of Y_{21}^F at $s = 0$ is proportional to $(p_1 + p_2)$ according to (7), it is necessary to have $p_2 = -p_1 = p > 0$. One can then use the value of Y_{21}^F at $s = 0$ to approximate the value of Y_{21}^F within the decoupling band. As illustrated by Fig. 2(c), the optimum Y_{21}^F that satisfies (3b) should be opposite to $j \cdot Im\{Y_{21}^A(0)\}$, that is:

$$\mathrm{Im}\left\{Y_{21}^F(s)\right\}\big|_{s\in[-j,j]} \approx \mathrm{Im}\left\{Y_{21}^F(0)\right\} = \gamma/p^2 = -\mathrm{Im}\left\{Y_{21}^A(0)\right\}. \tag{15}$$

In a general case where the imaginary part of Y_{21}^A could not be approximated by a constant over a certain frequency band, $p_2 \neq -p_1$ will result in a better decoupling bandwidth. An alternative choice is to introduce two finite transmission zeros in the CRDN such that the mutual coupling Y_{21}^A can be cancelled out in a broadband sense [18].

E. Design of Matching Network

To achieve a broadband impedance matching, $\mathrm{Re}\{Y_{11}\}(\mathrm{Re}\{Y_{22}\})$ should be the same as $\mathrm{Re}\{Y_{11}^A\}(\mathrm{Re}\{Y_{22}^A\})$ provided that $\mathrm{Im}\{Y_{11}\}(\mathrm{Im}\{Y_{22}\})$ approaches to zero in a broadband sense. From Fig. 2(d), it is observed that, in general, $\mathrm{Im}\{Y_{11}^A\}$ and $\mathrm{Im}\{Y_{22}^A\}$ can be different in terms of their slopes and zero locations. Therefore, to satisfy (5b) at the center frequency $(s = 0)$ for both ports, the following relations are obtained by setting $s = 0$ in (11a) and (11b):

$$Y_{11}^F(0) = j \cdot \frac{|\gamma|(d-c)}{2p^2} = -j \cdot \mathrm{Im}\left\{Y_{11}^A(0)\right\} \tag{16a}$$

$$Y_{22}^F(0) = j \cdot \frac{|\gamma|(d-c)}{2cdp^2} = -j \cdot \mathrm{Im}\left\{Y_{22}^A(0)\right\}. \tag{16b}$$

Since $c > 0$ and $d > 0$, it is obvious that

$$\mathrm{Im}\left\{Y_{11}^F(0)\right\} \cdot \mathrm{Im}\left\{Y_{22}^F(0)\right\} < 0 \tag{17}$$

which suggests that the center frequency ω_0 in (14) should be chosen in the way that $Y_{11}^A(0)$ and $Y_{22}^A(0)$ have different signs. Although this new ω_0 is different from the original center frequency of the antennas, two extra matching circuits can still be added to each port to match the decoupled antennas at the original center frequency. In this example, if $f_0 = \omega_0/2\pi$ is chosen to be 2.55 GHz, (16a) and (16b) can be satisfied simultaneously as shown in Fig. 2(d).

For a given antenna configuration, the slope of Y_{11}^A is an inherent characteristic depending on the Q value of the antenna. In order to optimally fulfill the impedance matching condition (5b), one needs to minimize the slope of Y_{11}^F at the resonant frequency and to use this slope information to represent the slope of Y_{11}^F within the decoupling frequency band. Closely examining the slope, one can find that it is inversely proportional to p^3. Therefore, a large p results in a small slope of Y_{11}^F within a frequency band and consequently good impedance matching can be obtained providing that a proper γ is chosen to achieve a good isolation according to (15). The same conclusion can be drawn for Y_{22}^F. Having had p chosen as large as the network realization allows, parameters γ, c, and d can be determined by (15) and (16). Consequently, the coupling coefficients in (12) can be obtained. It is also observed in Fig. 2(d) that when a CRDN is added to the original coupled antenna pair, in addition to an improved isolation, its radiation efficiency increases and, consequently, the matching bandwidth decreases. Like other decoupling techniques, this decoupling technique trades matching bandwidth for a better isolation and higher efficiency [22].

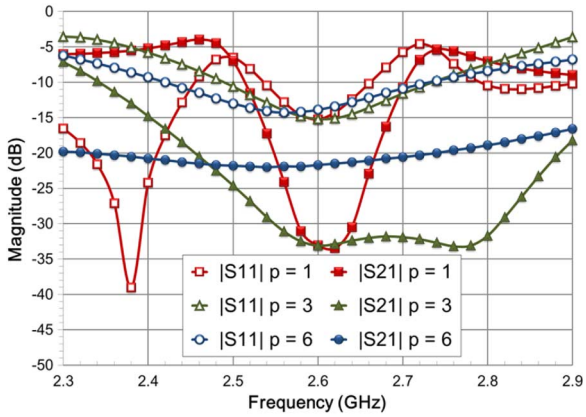

Fig. 3. Simulated $|S_{11}|$ and $|S_{21}|$ with different p values.

The importance of choosing a large p for broadband matching is studied parametrically and is presented in Fig. 3, where the circuit in Fig. 1 is used with the coupled antennas shown in Fig. 2. The decoupling bandwidths with $|\mathrm{S}_{11}| \leq -10$ dB and $|\mathrm{S}_{21}| \leq -20$ dB for $p = 1$, $p = 3$, and $p = 6$ are 112, 244, and 317 MHz, respectively. It is seen from (12) and (13) that the maximum p is stipulated by the maximum achievable inter-resonator coupling m_{12} when realizing a CRDN. Therefore, to obtain an optimum matching performance, it is advisable to maximize m_{12} when designing the decoupling network. For different realization technologies, such as microstrip and multilayer LTCC, the maximum realizable p can be quite different. It is interesting to observe from Fig. 3 that a tradeoff between the isolation level and the decoupling bandwidth can be made by choosing an appropriate value of parameter p.

III. Design Examples

Two examples are presented in this section. In both examples, printed monopole antenna elements are fabricated together with a CRDN on a double-sided FR4 substrate with relative dielectric constant of 4.3 and thickness of 1.6 mm. The center frequency is chosen to be 2.6 GHz (LTE Band 7). Full-wave electromagnetic simulations of these examples are performed by Agilent EMPro [23].

A. Example 1: A CRDN for an Asymmetric Array

The first example is to synthesize and design a CRDN for an asymmetric two-element array as shown in Fig. 2(a). The simulated and measured S-parameter of the original coupled but matched array is given in Fig. 2(b), in which an isolation of poorer than 8 dB at 2.6 GHz is observed.

A section of transmission line with its electric length determined by (6) is first introduced at each antenna port so that $\mathrm{Re}\{Y_{21}^A\} = 0$ at the center frequency. Fig. 2(c) shows the simulated Y_{21}^A in lowpass domain. Due to the in-house fabrication constraints, the minimum line width and spacing are limited to 0.2 mm. In this example p is designed to be 3. It can be seen from Fig. 2(c) that the imaginary part of Y_{21}^A is nearly a constant of -0.51 over a wide frequency band. According to (15), γ is found to be -4.59.

As shown in Fig. 2(d), the calculated $\mathrm{Im}\{Y_{11}^A(0)\} = -0.024$ and $\mathrm{Im}\{Y_{22}^A(0)\} = 0.034$. Therefore, using (16), c and d are found to be 0.7954 and 0.8895, respectively. Finally, with γ, p, c, and d determined, the coupling coefficients for the decoupling network are obtained from (12). The designed lowpass coupling matrix is listed in Table I with designed fractional bandwidth $\mathrm{FBW} = 10\%$.

TABLE I
Coupling Coefficients of Designed and Realized Decoupling Networks for Example 1 and Example 2 (Designed $\mathrm{FBW} = 10\%$)

	Designed (Example 1)	Realized (Example 1)	Designed (Example 2)	Realized (Example 2)
m_{S1}	1.1353	1.1315	1.2369	1.2421
m_{2L}	1.3497	1.2227	1.2369	1.2421
m_{12}	2.9953	3.0794	3.0000	2.7142
m_{11}	-0.1675	-0.1846	0.0000	0.0000
m_{22}	0.1675	0.1847	0.0000	0.0000

The coupling matrix is realized using two short-circuited and folded quarter-wavelength resonators with edge inter-resonator coupling. The input/output couplings are realized by the tapped-line configuration. The resonant frequency of each resonator is determined by the self-coupling. With appropriate layout design, the physical dimensions are tuned by comparing the extracted coupling coefficients to the synthesized ones until the overall responses match the desired one. Details on how to design a microstrip resonator and required couplings can be found in many text books [24].

The overall physical layout of the decoupled antenna array is shown in Fig. 4(a). Notice that two additional matching stubs are used to broaden the matching bandwidth. Fig. 4(b) shows the simulated and measured magnitudes of S-parameters of the decoupled array. The realized coupling matrix is extracted using the circuit model specified in Fig. 1 and is given in Table I as well for comparison. It is seen from Fig. 4(b) that the decoupling bandwidth with $|S_{21}| \leq -20$ dB is about 23% and the impedance matching bandwidth with $|S_{11}| \leq -10$ dB and $|S_{22}| \leq -10$ dB is about 9.2%. For the commonly accepted 6 dB return loss requirement for mobile terminals, the matching bandwidth of this decoupled array is about 15%.

To explain the working mechanism of this CRDN, EM simulated current distributions on the decoupled and the coupled arrays with excitation at port 1 are plotted in Fig. 5(a) and (b), respectively. It can be observed from Fig. 5(a) that the current induced by the antenna-to-antenna coupling at the terminated port (port 2) is well canceled by the current introduced through the CRDN.

B. Example 2: A CRDN for a Symmetric Array

The decoupling theory is applied to a symmetric array in this example, in which a pair of symmetric cone-shaped monopole antennas is considered. The ground size and substrate thickness are the same as those of example 1. The edge to edge spacing (S) between the two elements is 9.8 mm $(0.084\lambda_0)$.

For the symmetric array, a symmetric decoupling network can be synthesized and designed according to (13). The synthesized lowpass coupling matrix is listed in Table I. According to the coupling matrix, the physical dimensions of the resonators are determined and depicted in Fig. 6(a). Two extra matching stubs are added. Simulation and measurement results

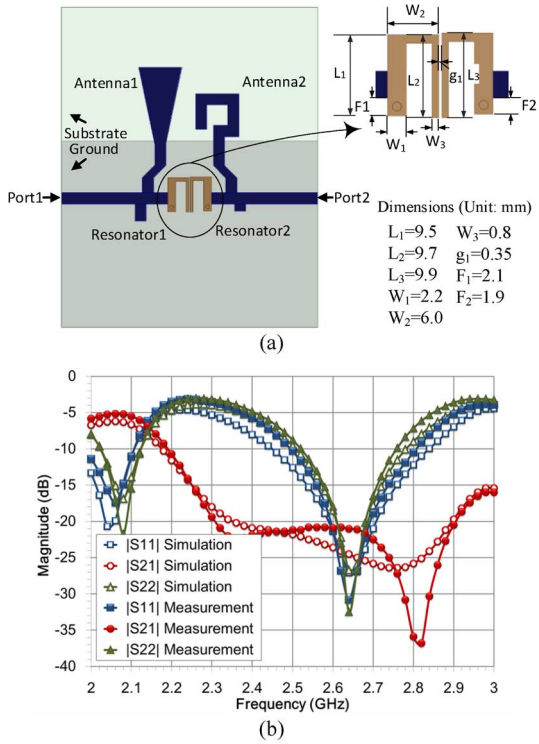

Fig. 4. (a) Layout of the decoupled asymmetric antenna array. (b) Simulated and measured responses of the decoupled array.

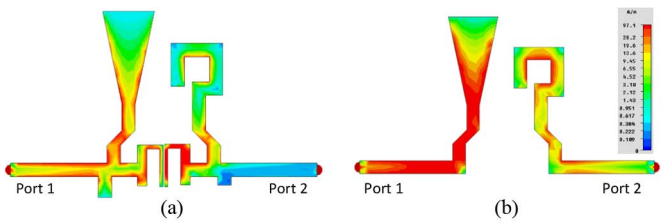

Fig. 5. (a) Current distributions of two antennas with a CRDN and (b) current distribution of the same antennas without a CRDN, when port 1 is excited.

are shown in Fig. 6(b) with the corresponding extracted coupling matrix listed in Table I. The decoupling bandwidth with $|S_{21}| \leq -20$ dB is about 15% and the matching bandwidth with $|S_{11}| \leq -6$ dB is about 19%.

C. Antenna Dependency and "One-Fit-All" Feature

In practice, the array form factors, such as inter-element spacing and ground plane size, affect the mutual admittance. Most of existing decoupling techniques require a complete redesign if any of the form factors are changed. However, a useful and practical feature of the CRDN technique is that only the input/output coupling coefficients m_{S1} and m_{2L} require to be modified to accommodate the change.

To demonstrate this feature, the properties of the mutual admittance of the symmetric array used in *Example 2* are intensively investigated by varying the spacing S from 4 to 112 mm and setting ground plane sizes to 54×72 mm^2 (SG) and 54×170 mm^2 (LG) using EM simulations. Three important conclusions can be drawn.

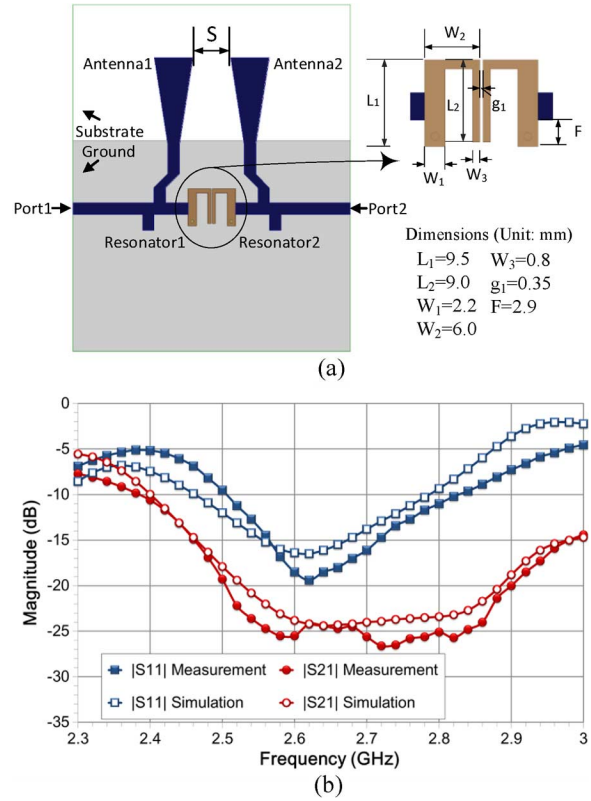

Fig. 6. (a) Layout of the decoupled symmetric antenna array. (b) Simulated and measured responses of the decoupled array.

1) In general, the isolation increases as the element spacing increases, however, the coupled arrays with the small ground (SG) are with better isolation as compared to those with the large ground (LG).
2) Both the real and imaginary parts of the mutual admittance are affected by the form factors that have to be considered in a design of a CRDN.
3) The larger the mutual coupling, the steeper the slope of the real part of mutual admittance versus frequency and the larger the imaginary part of the mutual admittance.

As revealed by (12) and (13), the same CRDN can be used to decouple a coupled array with different array form factors by keeping the same self-couplings for the resonators and the same inter-resonator coupling m_{12}. Only input/output couplings, i.e., m_{S1} and m_{2L}, need to be adjusted to accommodate the change in the form factors. For illustration, the circuit models of four CRDNs are designed to decouple the arrays with element spacing (S) of 8 and 22 mm, and the ground sizes of SG and LG, respectively. The designed coupling coefficients are listed in Table II. It can be seen that only the Input/Output couplings of a CRDN depend on the spacing and the ground size. Therefore, a "one-fit-all" module can be provided by consolidating all the circuitry parts except the I/O couplings, which can be adjusted as external components. This feature makes the CRDN technique very attractive.

IV. Performance Comparison in Practical Conditions

To have a thorough understanding of the performance of a CRDN in a practical implementation, several important figures

TABLE II
COUPLING COEFFICIENTS OF CRDNS FOR ARRAYS $1 \sim 4$ (FBW $= 10\%$)

	Array 1 S = 8, SG	Array 2 S = 8, LG	Array 3 S = 22, SG	Array 4 S = 22, LG
m_{S1}, m_{2L}	1.2156	1.5168	1.3913	1.6250
$\boldsymbol{m_{12}}$	**3.0000**	**3.0000**	**3.0000**	**3.0000**
m_{11}, m_{22}	0.0000	0.0000	0.0000	0.0000
20dB Isolation BW	411 (MHz)	183 (MHz)	312 (MHz)	177 (MHz)

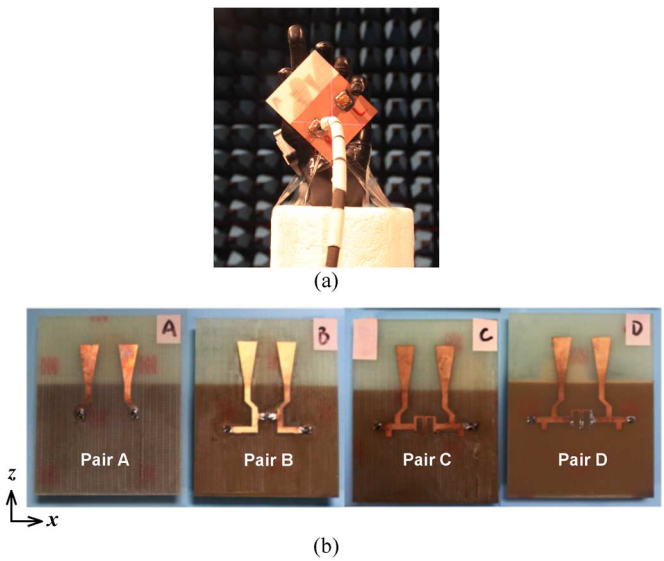

(a)

(b)

Fig. 7. (a) Hand phantom arrangement and measurements setup. (b) Four pairs of antennas under investigation.

of merit such as isolation, radiation patterns and radiation efficiencies, ECC and throughput are investigated both in free space and in the presence of a hand phantom.

The SPEAG hand phantom for mono-block phones SHO V2RB/LB is used[1] (see Fig. 7(a)). Four pairs of antennas are compared, including the symmetrical coupled cone-shaped antennas (Pair A), the same antennas decoupled by a lumped element designed by the procedure given in [9] (Pair B), the same antennas decoupled by a CRDN with wideband isolation of 20 dB (Pair C, CRDN 1) and the same antennas decoupled by a CRDN with isolation of 30 dB (Pair D, CRDN 2). All the prototypes are shown in Fig. 7(b). The radiation characteristics of these four pairs of antennas with and without hand phantom are measured using the in-house SATIMO SG128 spherical near-field scanner[2] in an ISO17025 accredited laboratory.

A. Matching and Isolation

The reflection and isolation coefficients of antenna pairs A, B, C, D with and without the presence of the hand phantom are examined and the results are displayed in Fig. 8. Since the hand phantom acts as a lossy dielectric medium in close proximity of the antennas, the resonant frequency of all the antenna pairs shifts to a lower value. However, the impact of the hand phantom on the isolation for the four antenna pairs seems to be

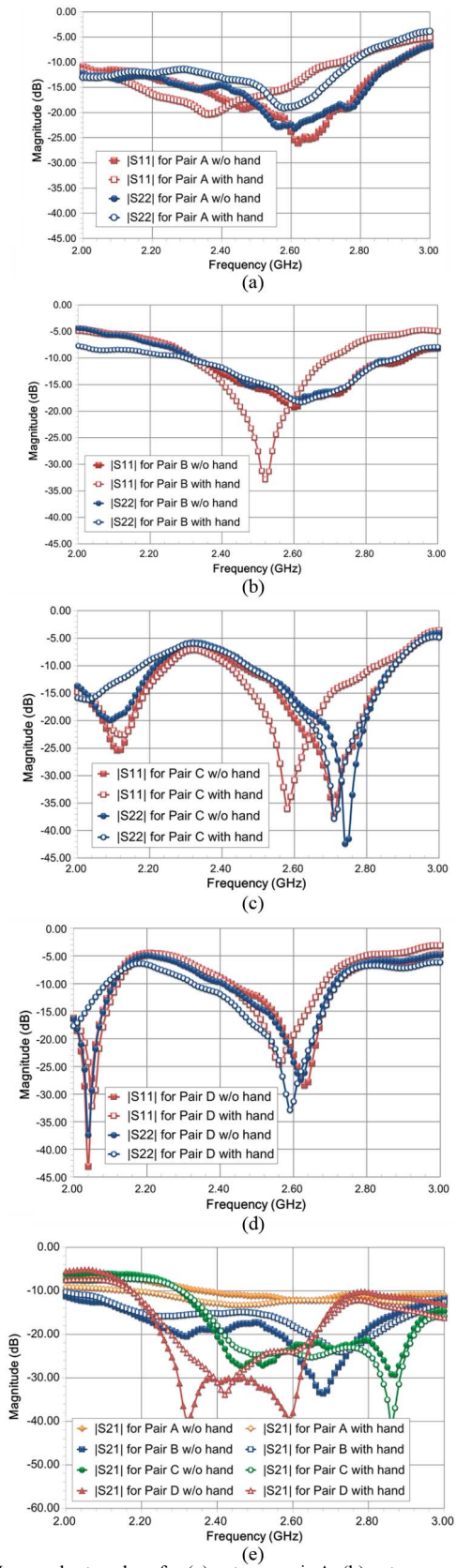

Fig. 8. Measured return loss for (a) antenna pair A, (b) antenna pair B, (c) antenna pair C, and (d) antenna pair D. (e) Measured isolation for antenna pairs A, B, C, and D.

quite different. For antenna pairs B, C, and D, the isolation increases in certain frequencies while it decreases in other

[1][Online]. Available: http://www.speag.com/

[2][Online]. Available: http://www.satimo.com/

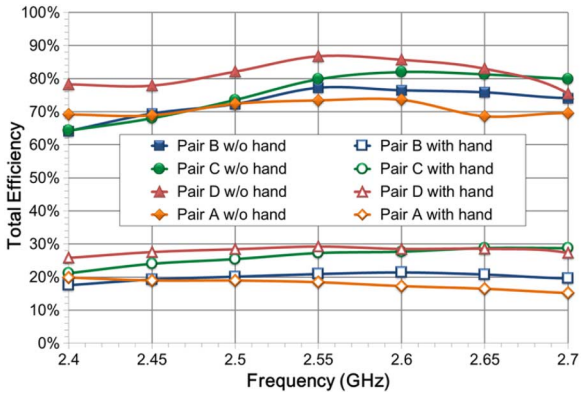

Fig. 9. Total efficiencies of four antenna pairs. (The efficiencies are averaged values of the two antennas for each pair.)

frequencies due to the detuning of resonance frequencies. Nevertheless, both pairs C and D achieve 20 dB isolation with a frequency band that is as wide as more than three times of that of pair B, with and without the presence of a hand phantom.

B. Radiation Efficiency

The total efficiencies of the antenna pairs are shown in Fig. 9. Under the free-space condition, the total efficiency for the coupled array (Pair A) is no more than 73% from 2.4 to 2.7 GHz, whereas for the decoupled array (Pair B), the efficiency is around 76% for the same band. For Pair C and Pair D using CRDNs, the typical efficiency has improved to 78% and 83%, respectively. Further improvements in efficiency can be expected if substrate with lower loss is used.

Due to the lossy nature of the hand phantom, the total efficiencies for all the four pairs of arrays have a huge degradation when the hand phantom is presented. Nevertheless, the Pair D still shows a significant efficiency improvement from 17% to 26% as compared to Pair A.

C. Envelope Correlation Coefficients (ECC)

The power patterns of the coupled array (Pair A) and one of the decoupled arrays (Pair C) are shown in Fig. 10. In the measurements, one of the antennas is excited while the other one is terminated by a 50 Ω load. Using the measured far-field vector phasor radiation patterns, the ECC of the each antenna pairs can be calculated by the method introduced in [25]. It is known that a lower envelope correlation leads to a higher channel capacity and a better diversity gain. For the decoupled antenna Pairs B, C, and D under the free space condition, an improvement in ECC from around 0.05 to smaller than 0.01 is seen in Fig. 11. But for the cases with the hand phantom, a much higher ECC is obtained for all the four pairs. This phenomenon is consistent with the discovery in [4] and [26]. For Pair A, the ECC increases to $0.17 \sim 0.27$ within the band of interest. Although the ECCs for Pair B, C, and D are also increased, the ECC for Pair D is below 0.025 from 2.4 to 2.7 GHz due to its wide band decoupling attribute.

D. Channel Capacity and Throughput

The channel capacities for an ideal 2-by-2 MIMO system using these four antenna arrays under different SNRs are calculated and are superposed in Fig. 12. The channel capacity calculation follows the method given in [27], which takes the antenna array efficiency and correlation into account. The transmitter antennas are assumed to be uncorrelated while all the arrays under investigation are placed at the receiver end. A larger enhancement of channel capacity is observed for cases having a hand phantom. An averaged improvement of around 1 bps/Hz is observed for Pair C and D as compared to Pair A.

According to COST Action 2100, throughput is suggested to be an important system level figure of merit [28]. However, to assess the throughput of a MIMO system in a given multipath environment is always challenging because it depends not only on the MIMO antenna array itself, but also on spatial and temporal characteristics of the radio channel as well as the space-time data processing algorithm. In this study, the two-stage method is adopted, which calculates the throughput using the passive antenna far-field pattern measurements and a MIMO channel model with appropriate parameters. Specifically, the WINNER II channel model in Agilent's W1715 MIMO Channel Builder of SystemVue is used [29]. The model is stochastic and geometry-based. The channel parameters for individual snapshots are based on the statistical distributions extracted from the channel measurement. The channel scenario B1 (Urban Micro-cell) is used in the throughput comparison of the four antenna pairs. The downlink transmitter is assumed to use a two-element linear array with omni-directional elements and half-wavelength spacing. The four antenna pairs under investigation are placed horizontally ($\theta = 0°$) at the receiver, facing the transmitter array in the broadside direction. The patterns of the antenna pairs are imported from measured results at 2.6 GHz. Other parameters are set to be the default values in the model. The fractional data throughputs, which are normalized with respect to their corresponding maximum achievable values, are superposed in Fig. 13.

E. Summary of the Performance Comparison

It can be concluded from the above performance evaluations and comparisons that the decoupled antenna arrays using different decoupling methods behave very differently with and without human interferences. There are huge degradations in efficiency, ECC, channel capacity and throughput in the presence of a hand phantom. However, despite the performance variations, the arrays with a CRDN outperform the original coupled array and the one with a lumped decoupling element. Moreover, the array with the CRDN that provides an isolation of 30 dB has the best performance among all the arrays under investigation. Therefore, it is worthwhile to design a compact array with a high isolated level, especially for mobile terminals in a realistic environment.

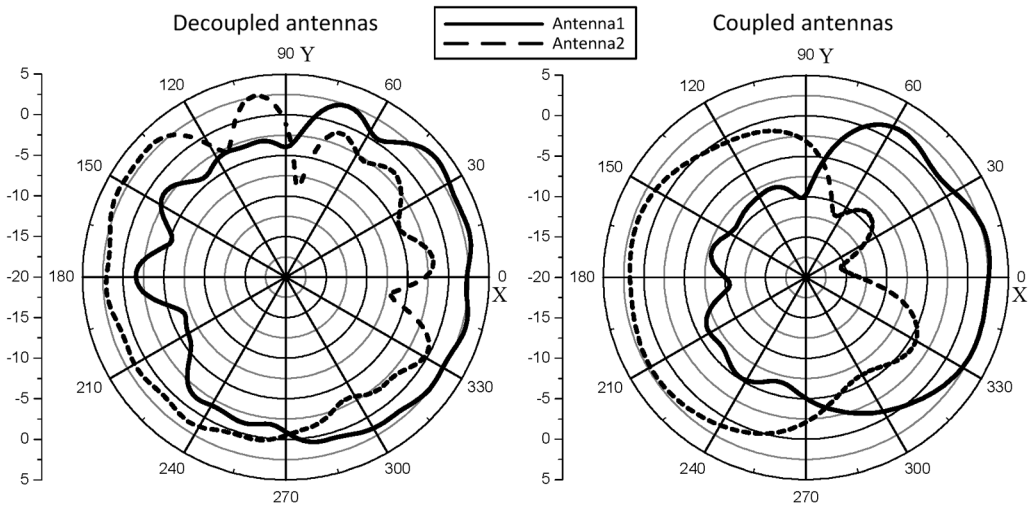

Fig. 10. Radiation patterns of the decoupled array-Pair C and the coupled array-Pair A in the xoy plane at 2.6 GHz.

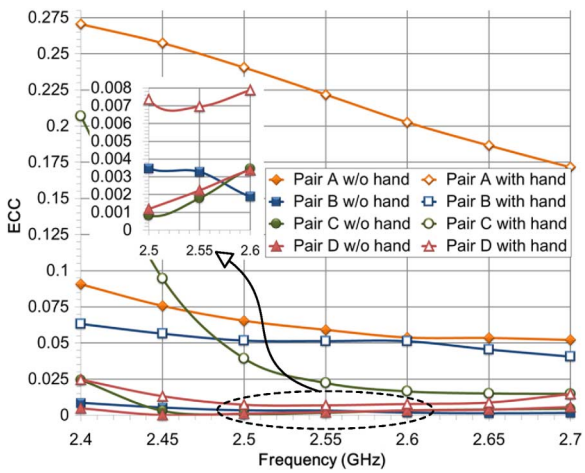

Fig. 11. Calculated envelope correlation coefficients for the four antenna pairs.

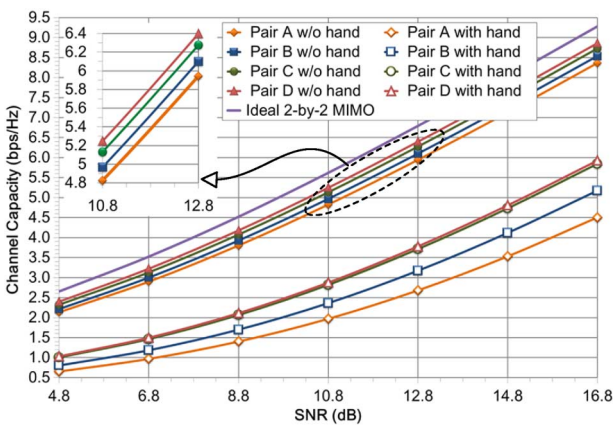

Fig. 12. Channel capacity for the four antenna arrays together with an ideal 2-by-2 MIMO array.

V. Conclusion

This paper proposed a new concept for decoupling two tightly coupled antennas using a coupled resonator network. The synthesis and design theory for the CRDN are also presented in detail. Starting from the measured admittance matrix of a pair of coupled antennas, the admittance functions of a coupled resonator decoupling network can be synthesized, which in turn leads to a 4-by-4 coupling matrix for a realizable circuit model. Several design examples using microstrip resonators on an FR4 substrate are also presented. More compact decoupling networks can be fabricated using advanced manufacturing technologies.

Simulated and experimental results have demonstrated that both port decoupling and matching can be achieved simultaneously over a relatively wide bandwidth by using a CRDN. It has also been shown through the measured radiation patterns that the decoupled antennas have a significant improvement in radiation efficiency, correlation coefficient, channel capacity, and above all throughput, both in free space and in the presence of a hand phantom. The examples have demonstrated a great potential of the proposed CRDN concept for mobile terminals that use MIMO or diversity antenna technology.

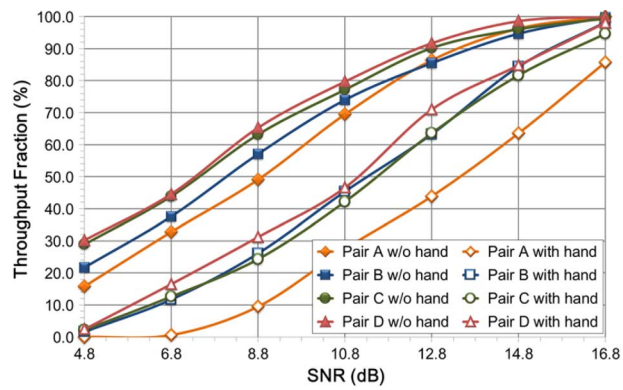

Fig. 13. Throughput fraction for the four antenna pairs without and with hand phantom in WINNER II channel model B1.

References

[1] G. L. Stuber, J. R. Barry, S. W. McLaughlin, Y. Li, M. A. Ingram, and T. G. Pratt, "Broadband MIMO-OFDM wireless communications," *Proc. IEEE*, vol. 92, no. 2, pp. 271–294, Feb. 2004.

[2] M. A. Jensen and J. W. Wallace, "A review of antennas and propagation for MIMO wireless communications," *IEEE Trans. Antennas Propag.*, vol. 52, no. 11, pp. 2810–2824, Nov. 2004.

[3] J. C. Coetzee and Y. Yu, "Port decoupling for small arrays by means of an eigenmode feed network," *IEEE Trans. Antennas Propag.*, vol. 56, no. 6, pp. 1587–1593, Jun. 2008.
[4] S. Zuo, Y.-Z. Yin, Y. Zhang, W.-J. Wu, and J.-J. Xie, "Eigenmode decoupling for MIMO loop-antenna based on 180 coupler," *Progr. Electromagn. Res. Lett.*, vol. 26, pp. 11–20, 2011.
[5] S. K. Chaudhury, H. J. Chaloupka, and A. Ziroff, "Multiport antenna Systems for MIMO and Diversity," presented at the EUCAP, Barcelona, Spain, Apr. 2010.
[6] C. Volmer, J. Weber, R. Stephan, K. Blau, and M. A. Hein, "An eigenanalysis of compact antenna arrays and its application to port decoupling," *IEEE Trans. Antennas Propag.*, vol. 56, no. 2, pp. 360–370, Feb. 2008.
[7] L. K. Yeung and Y. E. Wang, "Mode-based beamforming arrays for miniaturized platforms," *IEEE Trans. Microw. Theory Tech.*, vol. 57, no. 1, pp. 45–52, Jan. 2009.
[8] J. B. Andersen and H. H. Rasmussen, "Decoupling and descattering networks for antennas," *IEEE Trans. Antennas Propag.*, vol. 24, no. AP-6, pp. 841–846, Nov. 1976.
[9] S. Chang, Y.-S. Wang, and S.-J. Chung, "A decoupling technique for increasing the port isolation between strongly coupled antennas," *IEEE Trans. Antennas Propag.*, vol. 56, no. 12, pp. 3650–3658, Dec. 2008.
[10] C.-Y. Lui, Y.-S. Wang, and S.-J. Chung, "Two nearby dual-band antennas with high port isolation," presented at the IEEE Int. Symp. Antennas Propag., San Diego, CA, USA, Jul. 2008.
[11] A. Diallo, C. Luxey, P. L. Thuc, R. Staraj, and G. Kossiavas, "Study and reduction of the mutual coupling between two mobile phone PIFAs operating in the DCS1800 and UMTS bands," *IEEE Trans. Antennas Propag.*, vol. 54, no. 11, pp. 3063–3073, Nov. 2006.
[12] S.-W. Su, C.-T. Lee, and F.-S. Chang, "Printed MIMO-antenna system using neutralization-line technique for wireless USB-dongle applications," *IEEE Trans. Antennas Propag.*, vol. 60, no. 2, pp. 456–463, Feb. 2012.
[13] C. Luxey, "Design of multi-antenna systems for UTMS mobile phones," in *Proc. Loughborough Antennas Propag. Conf.*, Nov. 2009, pp. 57–64.
[14] F. Yang and Y. R. Samii, "Microstrip antennas integrated with electromagnetic band-gap EBG structures: A low mutual coupling design for array applications," *IEEE Trans. Antennas Propag.*, vol. 51, no. 10, pp. 2936–2946, Oct. 2003.
[15] C. Y. Chiu, C. H. Cheng, R. D. Murch, and C. R. Rowell, "Reduction of mutual coupling between closely-packed antenna element," *IEEE Trans. Antennas Propag.*, vol. 55, no. 6, pp. 1732–1738, Jun. 2007.
[16] M. M. Bait-Suwailam, M. S. Boybay, and O. M. Ramahi, "Electromagnetic coupling reduction in high-profile monopole antennas using single-negative magnetic metamaterials for MIMO applications," *IEEE Trans. Antennas Propag.*, vol. 58, no. 9, pp. 2894–2902, Sep. 2010.
[17] B. K. Lau and J. B. Andersen, "Simple and efficient decoupling of compact arrays with parasitic scatterers," *IEEE Trans. Antennas Propag.*, vol. 60, no. 2, pp. 464–472, Feb. 2012.
[18] L. Zhao, L. K. Yeung, and K.-L. Wu, "A novel second-order decoupling network for two-element compact antenna arrays," in *Proc. Asia-Pacific Microwave Conf.*, Dec. 2012, pp. 1172–1174.
[19] L. Zhao and K.-L. Wu, "A broadband coupled resonator decoupling network for a three-element compact array," presented at the IEEE MTT-S Int. Microw. Symp., Seattle, WA, USA, Jun. 2013.
[20] R. J. Cameron, C. M. Kudsia, and R. R. Mansour, *Microwave Filters for Communication systems*. New York, NY, USA: Wiley, 2007, ch. 6–8.
[21] M. E. van Valkenburg, *Network Analysis*. Englewood Cliffs, NJ, USA: Prentice-Hall, 1955.
[22] G. Shaker, S. Safavi-Naeini, and N. Sangary, "Q-Bandwidth relations for the design of coupled multi-element antennas," in *Proc. IEEE Antennas Propag. Soc. Int. Symp.*, Jun. 1–5, 2009, pp. 1–4.
[23] Agilent Technologies, Inc., Santa Clara, CA, USA, "EMPro 3D EM Simulation Software," Version 2012.09.
[24] J.-S. Hong and M. J. Lancaster, *Microstrip Filters for RF/Microwave Applications*, 2nd ed. New York, NY, USA: Wiley, 2011, ch. 7–10.
[25] R. G. Vaughan and J. B. Andersen, "Antenna diversity in mobile communications," *IEEE Trans. Veh. Technol.*, vol. VT-36, no. 4, pp. 147–172, Nov. 1987.
[26] B. Yanakiev, J. Ødum Nielsen, M. Christensen, and G. F. Pedersen, "On small terminal antenna correlation and impact on MIMO channel capacity," *IEEE Trans. Antennas Propag.*, vol. 60, no. 2, pp. 689–699, Feb. 2012.
[27] J. X. Yun and R. G. Vaughan, "Multiple element antenna efficiency and impact on diversity and capacity," *IEEE Trans. Antennas Propag.*, vol. 60, no. 2, pt. I, pp. 529–539, Feb. 2012.
[28] *Pervasive Mobile and Ambient Wireless Communications: COST Action 2100*, R. Verdone and A. Zanella, Eds. New York, NY, USA: Springer, 2012.
[29] Agilent Technologies, Inc., Santa Clara, CA, USA, "SystemVue Electronic System-Level (ESL) Design Software," Version 2013.01.

Luyu Zhao (S'09–M'14) was born in Xi'an, China, in 1984. He received the B.Eng. degree from Xidian University, Xi'an, China, in 2007, and is currently working toward the Ph.D. degree from The Chinese University of Hong Kong, Shatin, Hong Kong.

From 2007 to 2009, he was with the National Key Laboratory of Antennas and Microwave Technology, Xidian University, as a Research Assistant. His current research interests include design and application of multiple antennas for next generation mobile communication systems and passive RF and microwave components, circuits and systems.

Lap K. Yeung (S'00–M'02) received the B.Eng. degree in electrical and information engineering from University of Sydney, Sydney, Australia, in 1998, the M.Eng. degree in electronic engineering from The Chinese University of Hong Kong, Shatin, Hong Kong, in 2002, and the Ph.D. degree in electrical engineering from University of California at Los Angeles, Los Angeles, CA, USA, in 2009.

During 1999, he was with the Commonwealth Scientific and Industrial Research Organization (CSIRO), Sydney, Australia, where he was a research engineer involved in the numerical modeling of different antenna structures. From 2003 to 2006, he was with The Chinese University of Hong Kong, where he is involved in various LTCC multichip module (MCM) designs and the development of numerical algorithms for analyzing multilayer embedded RF modules.

Ke-Li Wu (M'90–SM'96–F'11) received the B.S. and M.Eng. degrees from the Nanjing University of Science and Technology, Nanjing, China, in 1982 and 1985, respectively, and the Ph.D. degree from Laval University, Quebec, QC, Canada, in 1989.

From 1989 to 1993, he was with the Communications Research Laboratory, McMaster University, as a Research Engineer and a Group Manager. In March 1993, he joined the Corporate R&D Division, COM DEV International, the largest Canadian space equipment manufacturer, where he was a Principal Member of Technical Staff. Since October 1999, he has been with The Chinese University of Hong Kong, Hong Kong, where he is a Professor and the Director of the Radiofrequency Radiation Research Laboratory (R3L). He has authored or coauthored numerous publications in the areas of EM modeling and microwave passive components, microwave filter and antenna engineering. His current research interests include partial element equivalent circuit (PEEC) and derived physically expressive circuit (DPEC) EM modeling of high speed circuits, RF and microwave passive circuits and systems, synthesis theory and practices of microwave filters, antennas for wireless terminals, LTCC-based multichip modules (MCMs), and RF identification (RFID) technologies. His research group is the main workforce in various active RFID research and applications in Hong Kong.

Prof. Wu is a member of IEEE MTT-8 subcommittee (Filters and Passive Components) and also serves as a TPC member for many prestigious international conferences including International Microwave Symposium. He was an Associate Editor of IEEE TRANSACTIONS ON MICROWAVE THEORY AND TECHNIQUES from 2006 to 2009. He was a recipient of the 1998 COM DEV Achievement Award for the development of exact EM design software of microwave filters and multiplexers and Asia Pacific Microwave Conference Prize in 2008 and 2012.